Computers and Mathematics with Applications 90 (2021) 55–65

Contents lists available at ScienceDirect

Computers and Mathematics with Applications

journal homepage: www.elsevier.com/locate/camwa

A mixture model for a dilute dispersion of gas in a liquid flow: Mathematical analysis and application to aluminium electrolysis

Emile Soutter, Jacques Rappaz, Marco Picasso *

Institute of Mathematics, EPFL, SB MATH, Station 8, 1015 Lausanne, Switzerland

ARTICLE INFO

Keywords:
Mixture model
Aluminium electrolysis
Diluted gas
Stabilized finite element approximation
Fluid with varying density

ABSTRACT

A mixture model to take into account the flow of small carbon dioxide bubbles dissolved in a liquid is presented. The model describes the evolution of the velocity fields (mixture and gas), the pressure and the volume fraction of gas. The system of equations is derived from mass and momentum conservation of the mixture and gas.

Well-posedness is proved for a simplified problem when the volume fraction of gas is known and small. A priori error estimates are proved for a stabilized finite element approximation.

An industrial application pertaining to aluminium electrolysis is presented. Numerical results indicated that the effect of gas bubbles on the flow cannot be neglected.

1. Introduction

According to [1], the carbon footprint of the aluminium production industry is 1.7% of global emissions from all sources, therefore huge efforts are done to enhance the process efficiency. In a Hall–Héroult cell dedicated to aluminium electrolysis, multi-scale (from millimetres to metres) and multi-physics (electromagnetic fields, immiscible fluids, gas bubbles of carbon dioxide, thermal gradients, alumina transport, chemical reactions) processes are involved in extreme conditions (high temperatures 950 °C, large currents 300 kA), so that numerical modelling is unavoidable [2–5].

In this paper, we focus on modelling the mixture flow at the level of the whole reduction cell. The effects of chemical reactions, thermal gradients, alumina transport are disregarded, the global effect of gas bubbles on the fluid flow is studied. Since the typical size of a gas bubble is a few millimetres whereas the size of a whole cell is several metres, a statistical averaged model is advocated, namely a dilute dispersion of gas bubbles in the liquid bath [6–8]. Unlike [4], effects such as nucleation or coalescence of bubbles are neglected, on the other side, our model can be easily incorporated in industrial simulations, for instance with the Alucell software [9–13].

The added value of this paper is twofold. First, well-posedness of a simplified model is proved. Assuming that the volume fraction of gas is prescribed, we analyse a modified Stokes problem with two velocities (mixture and gas) and one pressure. Under a smallness assumption of the volume fraction of gas, well-posedness can be proved, as well as a priori error estimates for a stabilized finite element approximation. Second, numerical results corresponding to the complete model are presented for an industrial simulation. The effect of gas bubbles on the average fluid flow for a whole reduction cell is discussed.

The outline is the following. In Section 2, the complete mathematical model for the velocities (gas, bath and mixture), volume fraction of gas and pressure is presented. In Section 3, well-posedness of a simplified stationary problem in which the volume fraction of gas is given and the viscous terms dominate is proved. In Section 4, convergence of a stabilized finite element approximation is performed. Section 5 is dedicated to numerical experiments, first for an academic problem to confirm the theoretical predictions for the simplified model, second for an industrial application pertaining to aluminium electrolysis.

2. The model

Let $\Omega \subset \mathbb{R}^d$, $d = 2, 3$, be the space domain occupied by the electrolytic bath with constant density ρ_b and the gas with constant density $\rho_g < \rho_b$. As already mentioned, gas is considered as a dispersed phase into the bath, α_g being the volume fraction of gas and μ_g its viscosity, similarly $(1 - \alpha_g)$ is the volume fraction of electrolytic bath and μ_b its viscosity.

Bath and gas are incompressible fluids with velocities $\boldsymbol{u}_b$, $\boldsymbol{u}_g$ and the same pressure p (the capillary pressure and surface tension forces are neglected). As in [7] the bath–gas mixture has density ρ_m and velocity $\boldsymbol{u}_m$ such that:

$$\rho_m = \alpha_g \rho_g + (1 - \alpha_g)\rho_b, \tag{1}$$

$$\rho_m \boldsymbol{u}_m = \alpha_g \rho_g \boldsymbol{u}_g + (1 - \alpha_g)\rho_b \boldsymbol{u}_b. \tag{2}$$

Let $\boldsymbol{F}$ denote the electromagnetic force field and $\boldsymbol{g}$ the gravity acceleration, then mass and momentum conservation of the bath–gas mixture

* Corresponding author.
E-mail addresses: emile.soutter@epfl.ch (E. Soutter), jacques.rappaz@epfl.ch (J. Rappaz), marco.picasso@epfl.ch (M. Picasso).

https://doi.org/10.1016/j.camwa.2021.03.007
Received 10 August 2020; Received in revised form 5 March 2021; Accepted 7 March 2021
Available online xxxx

yields:

$$\frac{\partial}{\partial t}(\rho_m \boldsymbol{u}_m) + \operatorname{div}(\rho_m \boldsymbol{u}_m \otimes \boldsymbol{u}_m) - \operatorname{div} \boldsymbol{\sigma}_m = \rho_m \boldsymbol{g} + \boldsymbol{F}, \tag{3}$$

$$\frac{\partial \rho_m}{\partial t} + \operatorname{div}(\rho_m \boldsymbol{u}_m) = 0, \tag{4}$$

where

$$\boldsymbol{\sigma}_m = 2\mu_m \epsilon(\boldsymbol{u}_m) - \frac{2}{d}\mu_m \operatorname{div} \boldsymbol{u}_m \boldsymbol{I} - p\boldsymbol{I}, \text{ and } \epsilon(\boldsymbol{u}_m) = \frac{\boldsymbol{\nabla u}_m + \boldsymbol{\nabla u}_m^T}{2}. \tag{5}$$

Here, for any vector field $\boldsymbol{u}$, $\boldsymbol{\nabla u}$ denotes the tensor with components $(\boldsymbol{\nabla u})_{i,j} = \partial u_i/\partial x_j$, $1 \le i, j \le d$ and $\boldsymbol{I}$ the identity tensor. Momentum conservation of the gas yields:

$$\frac{\partial}{\partial t}(\alpha_g \rho_g \boldsymbol{u}_g) + \operatorname{div}(\alpha_g \rho_g \boldsymbol{u}_g \otimes \boldsymbol{u}_g) = \operatorname{div} \boldsymbol{\tau}_g - \alpha_g \boldsymbol{\nabla} p + \alpha_g \rho_g \boldsymbol{g} + \boldsymbol{F}_D, \tag{6}$$

where

$$\boldsymbol{\tau}_g = 2\mu_g \epsilon(\boldsymbol{u}_g) - \frac{2}{d}\mu_g \operatorname{div} \boldsymbol{u}_g \boldsymbol{I}, \tag{7}$$

with the drag forces $\boldsymbol{F}_D = D\alpha_g(1-\alpha_g)(\boldsymbol{u}_b - \boldsymbol{u}_g)$, where D corresponds to Stokes' law, see Section 5.2 for details. Finally mass conservation of gas leads to:

$$\frac{\partial \alpha_g}{\partial t} + \operatorname{div}\left(\alpha_g \boldsymbol{u}_g\right) - \operatorname{div}(k \boldsymbol{\nabla} \alpha_g) = \dot{\alpha}_g, \tag{8}$$

where k is a diffusion coefficient, $\dot{\alpha}_g$ is the prescribed gas production per unit time due to the chemical reactions: it corresponds to alumina and carbon combining at the anodes which generates bubbles of carbon dioxide and pure aluminium:

$$2Al_2O_3 + 3C => 3CO_2 + 4Al. \tag{9}$$

Eqs. (3) (4) (6) (8) can be combined to obtain a system of equations where the unknowns are $\boldsymbol{u}_m, p, \boldsymbol{u}_g$ and α_g.

Remark 1. The viscosities μ_m and μ_g are constant in this model. In industrial applications [14], they follow a Smagorinski model, thus depend on the modulus of $\epsilon(\boldsymbol{u}_m)$.

3. Mathematical results on a simplified model

In the frame of the industrial process, the goal is to find a stationary solution as rapidly as possible. Numerical investigations have shown that an efficient strategy is to perform one time step of (8) in order to obtain a new α_g, then to solve the stationary equations corresponding to (3) (4) to obtain $\boldsymbol{u}_m$, p and finally solve the stationary equation corresponding to (6) to obtain $\boldsymbol{u}_g$. We therefore study the well-posedness of (3) (4) (6), α_g being a known quantity, and put aside Eq. (8) in our theoretical framework.

It is assumed that Ω is an open bounded domain in $\mathbb{R}^d$, $d = 2, 3$, with Lipschitz boundary $\partial\Omega$. The convective terms $\operatorname{div}(\rho_m \boldsymbol{u}_m \otimes \boldsymbol{u}_m)$ and $\operatorname{div}(\alpha_g \rho_g \boldsymbol{u}_g \otimes \boldsymbol{u}_g)$ in (3) and (6) are disregarded as diffusive terms dominate in the electrolysis application; they could be treated as perturbations as in [15] or incorporated in the analysis by making them part of the stress definition as in [16]. Eqs. (3) (4) (6) then simplify to:

$$-\operatorname{div}(\boldsymbol{\sigma}_m) = \rho_m \boldsymbol{g} + \boldsymbol{F}, \tag{10}$$

$$\operatorname{div}(\rho_m \boldsymbol{u}_m) = 0, \tag{11}$$

$$-\operatorname{div}(\boldsymbol{\tau}_g) = -\alpha_g \boldsymbol{\nabla} p + \alpha_g \rho_g \boldsymbol{g} + D\alpha_g(1-\alpha_g)(\boldsymbol{u}_b - \boldsymbol{u}_g), \tag{12}$$

where $\boldsymbol{\sigma}_m$ and $\boldsymbol{\tau}_g$ are given by (5) and (7) respectively. For the sake of simplicity we assume that μ_g and μ_m are positive constants and set $\boldsymbol{u}_g = \boldsymbol{u}_b = 0$ on $\partial\Omega$.

The notations for Sobolev spaces with their associated semi-norms and norms are the following. Let $K \subset \Omega$ be an open subdomain of Ω with Lipschitz boundary ∂K. For a d-index $s = (s_1, s_2) \in \mathbb{N}^2$ if $d = 2$ or $s = (s_1, s_2, s_3) \in \mathbb{N}^3$ if $d = 3$, and for a differentiable function $g : \mathbb{R}^d \to \mathbb{R}$, we denote by $|s| = \sum_{i=1}^d s_i$ et $D^s g = \partial^{|s|} g/(\Pi_{i=1}^d \partial x_i^{s_i})$. For $1 \le p < \infty$ and $0 \le m$:

$$W^{m,p}(K) = \{g \in L^p(K) : D^s g \in L^p(K), \ 1 \le |s| \le m, \},$$

and in the case where $m = 0$, $W^{0,p}(K) = L^p(K)$. We will also use

$$|g|_{m,p,K} = \Big(\sum_{|s|=m} \|D^s g\|^p_{L^p(K)}\Big)^{1/p} \text{ and } \|g\|_{m,p,K} = \Big(\sum_{|s|\le m} \|D^s g\|^p_{L^p(K)}\Big)^{1/p}.$$

When $p = 2$ we will use the notations $H^m(K) = W^{m,2}(K)$ and for $g \in H^m(K)$, the semi-norms $|g|_{m,K} = |g|_{m,2,K}$ and norms $\|g\|_{m,K} = \|g\|_{m,2,K}$. When $K = \Omega$, $H_0^m(\Omega)$ will denote the closure of all C^∞ functions with compact support $D(\Omega)$ in $H^m(\Omega)$. In this space, semi-norm $|.|_{m,\Omega}$ and norm $\|.\|_{m,\Omega}$ are equivalent. If $\boldsymbol{u} \in H^m(\Omega)^d$, we will denote $|\boldsymbol{u}|_{m,\Omega} = (\sum_{i=1}^d |u_i|^2_{m,\Omega})^{1/2}$ and $\|\boldsymbol{u}\|_{m,\Omega} = (\sum_{i=1}^d \|u_i\|^2_{m,\Omega})^{1/2}$. Finally, we will denote

$$L = \left\{ v \in L^2(\Omega) : \int_\Omega v \, dx = 0 \right\}, \text{ and } \boldsymbol{V} = H_0^1(\Omega)^d.$$

When $\boldsymbol{u}, \boldsymbol{v} \in \boldsymbol{V}$, the tensorial product $\epsilon(\boldsymbol{u}) : \epsilon(\boldsymbol{v})$ is given by

$$\epsilon(\boldsymbol{u}) : \epsilon(\boldsymbol{v}) = \sum_{i,j=1}^d \epsilon(\boldsymbol{u})_{i,j} \epsilon(\boldsymbol{v})_{i,j},$$

and $|\epsilon(\boldsymbol{u})| = (\epsilon(\boldsymbol{u}) : \epsilon(\boldsymbol{u}))^{1/2}$. The same notation is adopted for $\boldsymbol{\nabla u}$.

The weak form of Eqs. (10) and (11) is given by:

$$\int_\Omega 2\mu_m \left(\epsilon\left(\boldsymbol{u}_m\right) : \epsilon(\boldsymbol{v}) - \frac{1}{d} \operatorname{div} \boldsymbol{u}_m \operatorname{div} \boldsymbol{v} \right) dx - \int_\Omega p \operatorname{div} \boldsymbol{v} dx$$
$$= \int_\Omega \left(\rho_m \boldsymbol{g} + \boldsymbol{F}\right) . \boldsymbol{v} dx, \tag{13}$$

$$\int_\Omega \operatorname{div}(\rho_m \boldsymbol{u}_m) q dx = 0, \ \forall \boldsymbol{v} \in \boldsymbol{V}, \ \forall q \in L. \tag{14}$$

Remarking that $\alpha_g \boldsymbol{\nabla} p = \boldsymbol{\nabla}(\alpha_g p) - p \boldsymbol{\nabla} \alpha_g$ and $\boldsymbol{u}_b = (\rho_m \boldsymbol{u}_m - \alpha_g \rho_g \boldsymbol{u}_g)/(\rho_m - \alpha_g \rho_g)$ (see (2) and (1)), a weak form of (12) is

$$\int_\Omega 2\mu_g \left(\epsilon(\boldsymbol{u}_g) : \epsilon(\boldsymbol{v}) - \frac{1}{d} \operatorname{div} \boldsymbol{u}_g \operatorname{div} \boldsymbol{v} \right) dx + \int_\Omega D \frac{\alpha_g \rho_m}{\rho_b} \boldsymbol{u}_g . \boldsymbol{v} dx$$
$$= \int_\Omega p \boldsymbol{\nabla} \alpha_g . \boldsymbol{v} dx + \int_\Omega \alpha_g p \operatorname{div} \boldsymbol{v} dx + \int_\Omega \alpha_g (\rho_g \, \boldsymbol{g} + D \frac{\rho_m}{\rho_b} \boldsymbol{u}_m) . \boldsymbol{v} dx, \forall \boldsymbol{v} \in \boldsymbol{V}. \tag{15}$$

We are looking for $\boldsymbol{u}_m \in \boldsymbol{V}$, $p \in L$, $\boldsymbol{u}_g \in \boldsymbol{V}$ satisfying (13) to (15). We assume that $\boldsymbol{g} \in \mathbb{R}^d$, $\boldsymbol{F} \in L^2(\Omega)^d$ and $\alpha_g \in W^{1,3}(\Omega) \cap L^\infty(\Omega)$ is known and is such that $0 \le \alpha_g \le 1$. Using (1), it is obvious that $\rho_m \in W^{1,3}(\Omega) \cap L^\infty(\Omega)$, $\rho_g \le \rho_m \le \rho_b$, and

$$\frac{\partial \rho_m}{\partial x_i} = \frac{\partial \alpha_g}{\partial x_i} \left(\rho_g - \rho_b\right).$$

It should be noted that equations similar to (13) (14) have been analysed in [17,18] when the density of the mixture is known. In this paper, (15) is added to (13) (14) and the volume fraction of gas α_g is prescribed rather than the density of the mixture.

Lemma 1. *Assume $0 \le \alpha_g \le 1$ and $\alpha_g \in W^{1,3}(\Omega)$. The mapping $\boldsymbol{u} \in \boldsymbol{V} \to \rho_m \boldsymbol{u} \in \boldsymbol{V}$ (with ρ_m given by (1)) is an isomorphism. There exists two positive constants γ_1, γ_2 such that for every $\boldsymbol{u} \in \boldsymbol{V}$:*

$$|\boldsymbol{u}|_{1,\Omega} \le \gamma_1 (1 + \left|\alpha_g\right|_{1,3,\Omega}) \left|\rho_m \boldsymbol{u}\right|_{1,\Omega}, \tag{16}$$

$$\left|\rho_m \boldsymbol{u}\right|_{1,\Omega} \le \gamma_2 (1 + \left|\alpha_g\right|_{1,3,\Omega}) \left|\boldsymbol{u}\right|_{1,\Omega}. \tag{17}$$

Proof of Lemma 1. Let $\boldsymbol{u}$ be in $\boldsymbol{V}$ and let us compute the partial derivatives of $\boldsymbol{w} = \rho_m \boldsymbol{u}$.

We verify that $\boldsymbol{\nabla w} = \rho_m \boldsymbol{\nabla u} + \boldsymbol{u} \otimes \boldsymbol{\nabla} \rho_m$ with the notation $(\boldsymbol{a} \otimes \boldsymbol{b})_{i,j} = a_i b_j$.

By using (1) we have $\rho_g \le \rho_m \le \rho_b$ and $\boldsymbol{\nabla} \rho_m = \left(\rho_g - \rho_b\right) \boldsymbol{\nabla} \alpha_g$.

Hölder inequalities imply $\|\boldsymbol{\nabla w}\|_{0,\Omega} \le \rho_b \|\boldsymbol{\nabla u}\|_{0,\Omega} + C \|\boldsymbol{u}\|_{0,6,\Omega} \left\|\boldsymbol{\nabla} \alpha_g\right\|_{0,3,\Omega}$, where C is a constant independent of derivatives of the α_g. Since $H_0^1(\Omega) \hookrightarrow L^6(\Omega)$ with continuous embedding, we easily obtain (17).

In order to obtain (16), we use the same technique with

$$\boldsymbol{u} = \frac{1}{\rho_m} \boldsymbol{w}, \frac{1}{\rho_b} \le \frac{1}{\rho_m} \le \frac{1}{\rho_g} \text{ and } \boldsymbol{\nabla} \frac{1}{\rho_m} = -\frac{1}{\rho_m^2} \left(\rho_g - \rho_b\right) \boldsymbol{\nabla} \alpha_g. \quad \square$$

Remark 2. The assumption $\alpha_g \in W^{1,3}(\Omega)$ in Lemma 1 is sufficient for both dimensions $d = 2, 3$. When $d = 2$, it can be improved: $\alpha_g \in W^{1,2+k}(\Omega)$, with $k > 0$.

Lemma 2 (*Korn Equality*). *We assume $\boldsymbol{u} \in \boldsymbol{V}$. Then*

$$\int_\Omega |\epsilon(\boldsymbol{u})|^2\, dx = \frac{1}{2}\int_\Omega (|\boldsymbol{\nabla u}|^2 + |\operatorname{div} \boldsymbol{u}|^2) dx.$$

Proof of Lemma 2. Let $\boldsymbol{u}, \boldsymbol{v} \in D(\Omega)^d$. Then

$$\int_\Omega \epsilon(\boldsymbol{u}) : \epsilon(\boldsymbol{v}) dx = \int_\Omega \frac{1}{4}\sum_{i,j=1}^{d}\left(\frac{\partial u_i}{\partial x_j} + \frac{\partial u_j}{\partial x_i}\right)\left(\frac{\partial v_i}{\partial x_j} + \frac{\partial v_j}{\partial x_i}\right) dx =$$

$$\int_\Omega \frac{1}{4}\sum_{i,j=1}^{d}\left(\frac{\partial u_i}{\partial x_j}\frac{\partial v_i}{\partial x_j} + \frac{\partial u_j}{\partial x_i}\frac{\partial v_j}{\partial x_i} + 2\frac{\partial u_i}{\partial x_j}\frac{\partial v_j}{\partial x_i}\right) dx.$$

Integrating two times by part the last term, we obtain

$$\int_\Omega \frac{\partial u_i}{\partial x_j}.\frac{\partial v_j}{\partial x_i} dx = -\int_\Omega \frac{\partial^2 v_j}{\partial x_i \partial x_j} u_i dx = \int_\Omega \frac{\partial v_j}{\partial x_j}.\frac{\partial u_i}{\partial x_i} dx$$

and

$$\int_\Omega \epsilon(\boldsymbol{u}) : \epsilon(\boldsymbol{v}) dx = \frac{1}{2}\int_\Omega \boldsymbol{\nabla u} : \boldsymbol{\nabla v} dx + \frac{1}{2}\int_\Omega \operatorname{div}\boldsymbol{u}\, \operatorname{div}\boldsymbol{v}\, dx. \tag{18}$$

To complete the proof of this lemma, it is enough to remark that $D(\Omega)^d$ is dense in $\boldsymbol{V}$ and taking $\boldsymbol{v} = \boldsymbol{u}$. □

In order to solve Eqs. (13) and (14), we set $\boldsymbol{w} = \rho_m \boldsymbol{u}_m$ and we define two continuous bilinear forms $a : \boldsymbol{V} \times \boldsymbol{V} \to \mathbb{R}$ and $b : \boldsymbol{V} \times L \to \mathbb{R}$ by:

$$a(\boldsymbol{w}, \boldsymbol{v}) = \int_\Omega 2\mu_m \left(\epsilon\left(\frac{\boldsymbol{w}}{\rho_m}\right) : \epsilon(\boldsymbol{v}) - \frac{1}{d}\operatorname{div}\left(\frac{\boldsymbol{w}}{\rho_m}\right)\operatorname{div}(\boldsymbol{v})\right) dx, \tag{19}$$

$$\text{and } b(\boldsymbol{w}, q) = \int_\Omega \operatorname{div}\boldsymbol{w}\, q dx\,. \tag{20}$$

Remark that the bilinear form a is not symmetric and depends on α_g. With the change of variables $\boldsymbol{w} = \rho_m \boldsymbol{u}_m$, problem (13)–(14) is equivalent to find $\boldsymbol{w} \in \boldsymbol{V}$ and $p \in L$ satisfying

$$a(\boldsymbol{w}, \boldsymbol{v}) - b(\boldsymbol{v}, p) = \int_\Omega (\rho_m \boldsymbol{g} + \boldsymbol{F}).\boldsymbol{v} dx, \quad \forall \boldsymbol{v} \in \boldsymbol{V}, \tag{21}$$

$$b(\boldsymbol{w}, q) = 0 \quad \forall q \in L. \tag{22}$$

Notice that $\boldsymbol{w}$ belongs to the space:

$$\boldsymbol{V}_{div} = \{\boldsymbol{v} \in \boldsymbol{V} \,:\, \operatorname{div}(\boldsymbol{v}) = 0\}. \tag{23}$$

In order to analyse Eqs. (15), we define the continuous bilinear form $\ell : \boldsymbol{V} \times \boldsymbol{V} \to \mathbb{R}$ by:

$$\ell(\boldsymbol{u}, \boldsymbol{v}) = \int_\Omega 2\mu_g \left(\epsilon(\boldsymbol{u}) : \epsilon(\boldsymbol{v}) - \frac{1}{d}\operatorname{div}\boldsymbol{u}\ \operatorname{div}\boldsymbol{v}\right) dx + \int_\Omega D\frac{\alpha_g \rho_m}{\rho_b}\boldsymbol{u}.\boldsymbol{v} dx. \tag{24}$$

We prove

Lemma 3. *There exists $\varepsilon > 0$ such that if $\alpha_g \in W^{1,3}(\Omega)$, $\left|\alpha_g\right|_{1,3,\Omega} \le \varepsilon$ and $0 \le \alpha_g \le 1$, then the bilinear form $a(.,.)$ is coercive on $\boldsymbol{V}_{div}$.*

Proof of Lemma 3. Using Lemma 1, then $\boldsymbol{w} = \rho_m \boldsymbol{u}_m \in \boldsymbol{V}_{div}$ and, if $\left|\alpha_g\right|_{1,3,\Omega}$ is bounded, there exist two positive constants $\beta_1 < \beta_2$ satisfying

$$\beta_1 \left\|\boldsymbol{u}_m\right\|_{1,\Omega} \le \|\boldsymbol{w}\|_{1,\Omega} \le \beta_2 \left\|\boldsymbol{u}_m\right\|_{1,\Omega}. \tag{25}$$

It is easy to verify that

$$\epsilon\left(\frac{\boldsymbol{w}}{\rho_m}\right) = \frac{1}{\rho_m}\epsilon(\boldsymbol{w}) - \frac{1}{2\rho_m^2}\left(\boldsymbol{\nabla}\rho_m \otimes \boldsymbol{w} + \boldsymbol{w} \otimes \boldsymbol{\nabla}\rho_m\right),$$

when $(\boldsymbol{b} \otimes \boldsymbol{c})_{i,j} = b_i c_j$. It follows that for $\boldsymbol{w} \in \boldsymbol{V}_{div}$

$$a(\boldsymbol{w}, \boldsymbol{w}) = \int_\Omega \frac{2\mu_m}{\rho_m}\left(\epsilon(\boldsymbol{w}) : \epsilon(\boldsymbol{w}) - \frac{1}{d}\operatorname{div}\boldsymbol{w}\operatorname{div}\boldsymbol{w}\right) dx$$

$$- \int_\Omega \frac{\mu_m}{\rho_m^2}\left((\boldsymbol{\nabla}\rho_m \otimes \boldsymbol{w} + \boldsymbol{w} \otimes \boldsymbol{\nabla}\rho_m) : \epsilon(\boldsymbol{w})\right) dx \tag{26}$$

$$+ \int_\Omega \frac{2\mu_m}{d\rho_m^2}\left(\boldsymbol{w}.\boldsymbol{\nabla}\rho_m \operatorname{div}\boldsymbol{w}\right) dx.$$

By using Lemma 2 and the fact that $\operatorname{div}(\boldsymbol{w}) = 0$, there exists a constant C independent of $\boldsymbol{w}$ and $\boldsymbol{\nabla}\alpha_g$ such that

$$a(\boldsymbol{w}, \boldsymbol{w}) \ge \frac{\mu_m}{\rho_g}\left(|\boldsymbol{w}|_{1,\Omega}^2 - C\left\|\boldsymbol{\nabla}\rho_m\right\|_{0,3,\Omega}\|\boldsymbol{w}\|_{0,6,\Omega}|\boldsymbol{w}|_{1,\Omega}\right).$$

It is sufficient to remark that $H_0^1(\Omega) \hookrightarrow L^6(\Omega)$ with continuous embedding, that $\boldsymbol{\nabla}\rho_m = (\rho_g - \rho_b)\boldsymbol{\nabla}\alpha_g$, that $|.|_{1,\Omega}$ is equivalent to $\|.\|_{1,\Omega}$ in $H_0^1(\Omega)$, in order to prove that if $\left|\alpha_g\right|_{1,3,\Omega}$ is small enough, then the bilinear form $a(.,.)$ is uniformly coercive on $\boldsymbol{V}_{div}$. □

Proposition 1. *There exists $\varepsilon > 0$ such that if $\alpha_g \in W^{1,3}(\Omega)$, $\left|\alpha_g\right|_{1,3,\Omega} \le \varepsilon$ and $0 \le \alpha_g \le 1$, then Problem (13)–(14), in which ρ_m is defined by (1), possesses a unique solution $(\boldsymbol{u}_m, p) \in \boldsymbol{V} \times L$. Moreover there exists a constant C such that $\left\|\boldsymbol{u}_m\right\|_{1,\Omega} + \|p\|_{0,\Omega} \le C$.*

Proof of Proposition 1. The usual inf–sup condition on $b(.,.)$, together with the previous lemma implies (see [19] for instance) the existence and uniqueness of $(\boldsymbol{w}, p) \in \boldsymbol{V} \times L$ for Eqs. (21) and (22). By setting $\boldsymbol{u}_m = \boldsymbol{w}/\rho_m$ and using (25), we can conclude. □

Proposition 2. *There exists $\varepsilon > 0$ such that if $\alpha_g \in W^{1,3}(\Omega)$, $\left|\alpha_g\right|_{1,3,\Omega} \le \varepsilon$ and $0 \le \alpha_g \le 1$, then Problem (15) possesses a unique solution $\boldsymbol{u}_g \in \boldsymbol{V}$. Moreover there exists a constant C (independent of α_g) such that $\left\|\boldsymbol{u}_g\right\|_1 \le C$.*

Proof of Proposition 2. Clearly, using Lemma 2 and the hypotheses of this Proposition, we show that the bilinear form ℓ defined by (24) is coercive and continuous on $\boldsymbol{V} \times \boldsymbol{V}$.

In order to finish the proof of this Proposition, it remains to prove that the right-hand side of (15) is bounded for every $\boldsymbol{v} \in H_0^1(\Omega)$, $\|\boldsymbol{v}\|_{1,\Omega} = 1$.

By estimating the three integrals of the right-hand side of (15), using Hölder inequalities and hypotheses of this Proposition, we successively obtain:

$$\left|\int_\Omega p\nabla\alpha_g.\boldsymbol{v} dx\right| \le \varepsilon\|p\|_{0,\Omega}\|\boldsymbol{v}\|_{0,6,\Omega};$$

$$\left|\int_\Omega \alpha_g p \operatorname{div}\boldsymbol{v} dx\right| \le \|p\|_{0,\Omega}\|\boldsymbol{v}\|_{1,\Omega};$$

$$\left|\int_\Omega (\alpha_g \rho_g\, \boldsymbol{g} + D\frac{\alpha_g \rho_m}{\rho_b}\boldsymbol{u}_m).\boldsymbol{v} dx\right| \le (\rho_g|\boldsymbol{g}| + D\left\|\boldsymbol{u}_m\right\|_{0,\Omega})\|\boldsymbol{v}\|_{0,\Omega}.$$

Using again the embedding $H_0^1(\Omega) \hookrightarrow L^6(\Omega)$, we can conclude. □

In this section we have therefore proved that if $\alpha_g : \Omega \to \mathbb{R}$ is given such that $0 \le \alpha_g \le 1$, $\alpha_g \in W^{1,3}(\Omega)$ with $\left|\alpha_g\right|_{1,3,\Omega}$ small enough,[1] then Problem (13) to (15) has a unique solution.

4. Numerical approximation

Let us assume that Ω is a polygonal ($d = 2$) or polyhedral domain ($d = 3$). For any $h > 0$, let $\mathcal{T}_h$ be a conformal regular triangular/tetrahedral mesh of $\overline{\Omega}$ with triangles/tetrahedra $K \in \mathcal{T}_h$ with diameter $h_K \le h$.

$$W_h = \{q \in C^0\left(\overline{\Omega}\right) \,:\, q_{/K} \in \mathbb{P}_1(K), \forall K \in \mathcal{T}_h\}, \tag{27}$$

where $\mathbb{P}_1(K)$ denotes the set of polynomials of degree 1 on K. Let $P_1, P_2, \ldots P_{N_h}$ be the nodes of the triangular/tetrahedral mesh $\mathcal{T}_h$, and let $\varphi_1, \varphi_2, \ldots \varphi_{N_h}$ the finite element basis of W_h.

[1] In 2D ($d = 2$), if $\alpha_g \in W^{1,s}(\Omega)$, $s > 2$ with $|\alpha_g|_{1,s,\Omega}$ small enough.

If $q \in C^0(\overline{\Omega})$ we denote by $\pi_h q$ its Lagrange interpolation on W_h, i.e

$$\pi_h q = \sum_{j=1}^{N_h} q(P_j)\varphi_j.$$

Now we define

$$\boldsymbol{V}_h = \boldsymbol{V} \cap W_h^d, \text{ and } L_h = L \cap W_h.$$

For a function $\boldsymbol{v} \in C^0(\overline{\Omega})^d$ such that $\boldsymbol{v} = \boldsymbol{0}$ on $\partial\Omega$, we denote by $\Pi_h \boldsymbol{v}$ its interpolation on $\boldsymbol{V}_h$, i.e.

$$\Pi_h \boldsymbol{v} = \sum_{j=1}^{N_h} \boldsymbol{v}(P_j)\varphi_j.$$

Recall the properties of the Lagrange interpolation (for instance [20]): $\forall f \in H^2(\Omega)$, there is a constant c such that:

$$\|f - \Pi_h f\|_{1,\Omega} \le ch|f|_{2,\Omega}, \ \forall h > 0. \tag{28}$$

An approximation of Problems (13) (14) and (15) will be: find $(\boldsymbol{u}_{m,h}, p_h, \boldsymbol{u}_{g,h}) \in \boldsymbol{V}_h \times L_h \times \boldsymbol{V}_h$ such that for every $\boldsymbol{v} \in \boldsymbol{V}_h$, $q \in L_h$ we have

$$\int_\Omega 2\mu_m \left(\epsilon(\boldsymbol{u}_{m,h}) : \epsilon(\boldsymbol{v}) - \frac{1}{d} \operatorname{div} \boldsymbol{u}_{m,h} \operatorname{div} \boldsymbol{v} \right) dx$$
$$- \int_\Omega p_h \operatorname{div} \boldsymbol{v} dx = \int_\Omega (\rho_m \boldsymbol{g} + \boldsymbol{F}).\boldsymbol{v} dx, \tag{29}$$

$$\int_\Omega \operatorname{div} \left(\Pi_h \left(\rho_m \boldsymbol{u}_{m,h} \right) \right) q dx + \beta h^2 \int_\Omega \boldsymbol{\nabla} p_h . \boldsymbol{\nabla} q dx = 0, \tag{30}$$

$$\int_\Omega 2\mu_g \left(\epsilon(\boldsymbol{u}_{g,h}) : \epsilon(\boldsymbol{v}) - \frac{1}{d} \operatorname{div} \boldsymbol{u}_{g,h} \operatorname{div} \boldsymbol{v} \right) dx + \int_\Omega D \frac{\alpha_g \rho_m}{\rho_b} \boldsymbol{u}_{g,h}.\boldsymbol{v} dx \tag{31}$$
$$= \int_\Omega p_h \boldsymbol{\nabla} \alpha_g . \boldsymbol{v} dx + \int_\Omega \alpha_g p_h \operatorname{div} \boldsymbol{v} dx + \int_\Omega (\alpha_g \rho_g \, \boldsymbol{g} + D \frac{\alpha_g \rho_m}{\rho_b} \boldsymbol{u}_{m,h}).\boldsymbol{v} dx.$$

The stabilization term $\beta h^2 \int_\Omega \boldsymbol{\nabla} p_h . \boldsymbol{\nabla} q \ dx$ in (30) is added for stability purposes [21], in our simulations we have used $\beta = \rho_b / \mu_b$. Note that in (30), we have replaced $\rho_m \boldsymbol{u}_{m,h}$ by $\Pi_h(\rho_m \boldsymbol{u}_{m,h})$ to take into account quadrature formula.

In order to analyse Eqs. (29) (30), we proceed as in Lemma 1 by introducing the variable

$$\boldsymbol{w}_h = \Pi_h(\rho_m \boldsymbol{u}_{m,h}). \tag{32}$$

Clearly we have

$$\boldsymbol{u}_{m,h} = \Pi_h(\boldsymbol{w}_h / \rho_m), \tag{33}$$

so that setting

$$a_h(\boldsymbol{w}_h, \boldsymbol{v}) = \int_\Omega 2\mu_m \left(\epsilon(\Pi_h(\boldsymbol{w}_h/\rho_m)) : \epsilon(\boldsymbol{v}) - \frac{1}{d} \operatorname{div}(\Pi_h(\boldsymbol{w}_h/\rho_m)) \operatorname{div} \boldsymbol{v} \right) dx,$$

problem (29) (30) is equivalent to find $\boldsymbol{w}_h \in \boldsymbol{V}_h$ and $p_h \in L_h$ such that for every $\boldsymbol{v} \in \boldsymbol{V}_h$ and $q \in L_h$ we have

$$a_h(\boldsymbol{w}_h, \boldsymbol{v}) - b(\boldsymbol{v}, p_h) = \int_\Omega (\rho_m \boldsymbol{g} + \boldsymbol{F}).\boldsymbol{v} dx, \tag{34}$$

$$b(\boldsymbol{w}_h, q) + \beta h^2 \int_\Omega \boldsymbol{\nabla} p_h . \boldsymbol{\nabla} q dx = 0. \tag{35}$$

In order to prove convergence of the solutions of (34) (35) towards that of (21) (22), we establish three lemmas.

Lemma 4. *Let $\rho \in W^{2,3}(\Omega) \cap W^{1,\infty}(\Omega)$. Then there exists a constant C such that*

$$\left\| \rho q - \pi_h(\rho q) \right\|_{1,\Omega} \le Ch \|q\|_{1,\Omega} \ \forall q \in W_h. \tag{36}$$

Proof of Lemma 4. Clearly, if $\rho \in W^{2,3}(\Omega) \cap W^{1,\infty}(\Omega)$ and $q \in W_h$, then $\rho q \in H^1(\Omega)$ and $\rho q_{/K} \in H^2(K)$, $\forall K \in \Gamma_h$. It is well known (see [20]) that the following estimate holds:

$$\left\| \rho q - \pi_h(\rho q) \right\|_{1,\Omega}^2 \le Ch^2 \sum_{K \in \Gamma_h} |\rho q|_{2,K}^2 . \tag{37}$$

When $q \in W_h$, then $\partial^2 q / \partial x_i \partial x_j = 0$ on K and

$$\frac{\partial^2(\rho q)}{\partial x_i \partial x_j} = \frac{\partial^2 \rho}{\partial x_i \partial x_j} q + \frac{\partial \rho}{\partial x_i} \frac{\partial q}{\partial x_j} + \frac{\partial \rho}{\partial x_j} \frac{\partial q}{\partial x_i}.$$

Consequently

$$\left\| \frac{\partial^2(\rho q)}{\partial x_i \partial x_j} \right\|_{0,K}^2 \le \left\| \frac{\partial^2 \rho}{\partial x_i \partial x_j} \right\|_{0,3,K}^2 \|q\|_{0,6,K}^2 + \left\| \frac{\partial \rho}{\partial x_i} \right\|_{0,\infty,K}^2 \left\| \frac{\partial q}{\partial x_j} \right\|_{0,K}^2$$
$$+ \left\| \frac{\partial \rho}{\partial x_j} \right\|_{0,\infty,K}^2 \left\| \frac{\partial q}{\partial x_i} \right\|_{0,K}^2$$
$$\le C \left(|\rho|_{2,3,K}^2 \|q\|_{0,6,K}^2 + |\rho|_{1,\infty,K}^2 |q|_{1,K}^2 \right).$$

Since $\|q\|_{0,6,K} \le C \|q\|_{1,K}$, then (37) allows to conclude. □

The equivalent discrete proposition of Lemma 1 can be stated.

Lemma 5. *Assume $0 \le \alpha_g \le 1$ and $\alpha_g \in W^{2,3}(\Omega) \cap W^{1,\infty}(\Omega)$. When ρ_m is given by (1), the application $T_h : \boldsymbol{V}_h \to \boldsymbol{V}_h$ defined by*

$$T_h(\boldsymbol{\omega}) = \Pi_h(\rho_m \boldsymbol{\omega}), \ \forall \boldsymbol{\omega} \in \boldsymbol{V}_h \tag{38}$$

is an isomorphism of $\boldsymbol{V}_h$ uniformly in h, i.e, there exist two positive constants C_1 and C_2 such that

$$C_1 \|\boldsymbol{\omega}\|_{1,\Omega} \le \left\| T_h(\boldsymbol{\omega}) \right\|_{1,\Omega} \le C_2 \|\boldsymbol{\omega}\|_{1,\Omega} \ \forall \boldsymbol{\omega} \in \boldsymbol{V}_h. \tag{39}$$

Thus we have $T_h^{-1}(\boldsymbol{u}) = \Pi_h(\rho_m^{-1} \boldsymbol{u}), \ \forall \boldsymbol{u} \in \boldsymbol{V}_h$.

Proof of Lemma 5. We have, using Lemma 4:

$$\left\| \Pi_h(\rho_m \boldsymbol{\omega}) \right\|_{1,\Omega} \le \left\| \Pi_h(\rho_m \boldsymbol{\omega}) - \rho_m \boldsymbol{\omega} \right\|_{1,\Omega} + \left\| \rho_m \boldsymbol{\omega} \right\|_{1,\Omega}$$
$$\le Ch \|\boldsymbol{\omega}\|_{1,\Omega} + \left\| \rho_m \right\|_{1,\infty,\Omega} \|\boldsymbol{\omega}\|_{1,\Omega}.$$

The same applies to ρ_m^{-1} instead of ρ_m. □

Lemma 6. *Under the assumptions of Lemma 5, there exists a constant $C > 0$ such that*

$$|a(\boldsymbol{\varphi}, \boldsymbol{\psi}) - a_h(\boldsymbol{\varphi}, \boldsymbol{\psi})| \le Ch \|\boldsymbol{\varphi}\|_{1,\Omega} \|\boldsymbol{\psi}\|_{1,\Omega} \ \forall \boldsymbol{\varphi}, \boldsymbol{\psi} \in \boldsymbol{V}_h.$$

Proof of Lemma 6. By bilinearity of a and a_h we get $\forall \boldsymbol{\varphi}, \boldsymbol{\psi} \in \boldsymbol{V}_h$:

$$\left| a(\boldsymbol{\varphi}, \boldsymbol{\psi}) - a_h(\boldsymbol{\varphi}, \boldsymbol{\psi}) \right| =$$
$$\left| 2\mu_m \int_\Omega \left(\epsilon \left(\frac{\boldsymbol{\varphi}}{\rho_m} - \Pi_h \left(\frac{\boldsymbol{\varphi}}{\rho_m} \right) \right) : \epsilon(\boldsymbol{\psi}) - \frac{1}{d} \operatorname{div} \left(\frac{\boldsymbol{\varphi}}{\rho_m} - \Pi_h \left(\frac{\boldsymbol{\varphi}}{\rho_m} \right) \right) \operatorname{div} \boldsymbol{\psi} \right) dx \right|.$$

Using Lemma 4, there exists two constants C_1, C_2 such that

$$\left| a(\boldsymbol{\varphi}, \boldsymbol{\psi}) - a_h(\boldsymbol{\varphi}, \boldsymbol{\psi}) \right| \le C_1 \left\| \frac{\boldsymbol{\varphi}}{\rho_m} - \Pi_h(\frac{\boldsymbol{\varphi}}{\rho_m}) \right\|_{1,\Omega} \|\boldsymbol{\psi}\|_{1,\Omega}$$
$$\le C_2 h \|\boldsymbol{\varphi}\|_{1,\Omega} \|\boldsymbol{\psi}\|_{1,\Omega}. \quad \square$$

Corollary 1. *Assume $0 \le \alpha_g \le 1$ and $\alpha_g \in W^{2,3}(\Omega) \cap W^{1,\infty}(\Omega)$, and let $\epsilon > 0$ be such as in Lemma 3. Then there exists $h_0 > 0$ such that if $h \le h_0$, Problem (34) (35) possesses a unique solution $(\boldsymbol{w}_h, p_h) \in \boldsymbol{V}_h \times L_h$. Moreover there exists a constant C (independent of h) such that $\|\boldsymbol{w}_h\|_{1,\Omega} + h \left\| \boldsymbol{\nabla} p_h \right\|_{0,\Omega} \le C$.*

Proof of Corollary 1. Under these assumptions, Lemmas 6 and 3 imply that the bilinear form $a_h(.,.)$ is uniformly coercive on $\boldsymbol{V}_h$ when $h \le h_0$ is small enough, i.e there exists $\kappa > 0$ such that if $h \le h_0$

$$a_h(\boldsymbol{\varphi}, \boldsymbol{\varphi}) \ge \kappa \|\boldsymbol{\varphi}\|_{1,\Omega}^2, \ \forall \boldsymbol{\varphi} \in \boldsymbol{V}_h. \tag{40}$$

Setting $A((\boldsymbol{w},p);(\boldsymbol{v},q)) = a_h(\boldsymbol{w},\boldsymbol{v}) - b(\boldsymbol{v},p) + b(\boldsymbol{w},q) + \beta h^2 \int_\Omega \boldsymbol{\nabla} p.\boldsymbol{\nabla} q dx$, it follows that $A : \left(\boldsymbol{V}_h \times L_h\right) \times \left(\boldsymbol{V}_h \times L_h\right) \to \mathbb{R}$ is coercive on $\boldsymbol{V}_h \times L_h$ provided with the norm $\|\boldsymbol{w}\|_{1,\Omega} + h\|\boldsymbol{\nabla} p\|_{0,\Omega}$, i.e:

$$A((\boldsymbol{w},p);(\boldsymbol{w},p)) \geq \kappa \|\boldsymbol{w}\|_{1,\Omega}^2 + \beta h^2 \|\boldsymbol{\nabla} p\|_{0,\Omega}^2, \ \forall (\boldsymbol{w},p) \in \boldsymbol{V}_h \times L_h.$$

The proof of this corollary is a consequence of the equivalence of Problem (34) (35) with $A((\boldsymbol{w}_h,p_h);(\boldsymbol{v},q)) = \int_\Omega (\rho_m \boldsymbol{g} + \boldsymbol{F}).\boldsymbol{v} dx$ for every $(\boldsymbol{v},q) \in \boldsymbol{V}_h \times L_h$. □

We now derive error estimates between $(\boldsymbol{w},p)$ and $(\boldsymbol{w}_h,p_h)$ and, consequently, between $\boldsymbol{u}_m$ and $\boldsymbol{u}_{m,h}$. To do this we assume that the solution of Problem (13) (14) satisfies

$$(\boldsymbol{u}_m,p) \in H^2(\Omega)^d \times H^1(\Omega). \tag{41}$$

Let us remark that if assumption (41) is true and if $\alpha_g \in W^{2,3}(\Omega) \cap W^{1,\infty}(\Omega)$, then $(\boldsymbol{w},p) \in H^2(\Omega)^d \times H^1(\Omega)$ when $\boldsymbol{w} = \rho_m \boldsymbol{u}_m$.

Proposition 3. *Under the assumptions of Corollary 1 and (41), there exists a constant C independent of h such that*

$$\left\|\boldsymbol{u}_m - \boldsymbol{u}_{m,h}\right\|_{1,\Omega} + h\left\|\boldsymbol{\nabla}\left(p - p_h\right)\right\|_{0,\Omega} \leq Ch. \tag{42}$$

Proof of Proposition 3. By subtraction of (34) to (21), we obtain for every $\boldsymbol{v} \in \boldsymbol{V}_h$:

$$a(\boldsymbol{w} - \boldsymbol{w}_h, \boldsymbol{v}) - b(\boldsymbol{v}, p - p_h) = a_h(\boldsymbol{w}_h, \boldsymbol{v}) - a(\boldsymbol{w}_h, \boldsymbol{v}), \tag{43}$$

and consequently:

$$\begin{aligned} &a(\boldsymbol{w} - \boldsymbol{w}_h, \boldsymbol{w} - \boldsymbol{w}_h) - b(\boldsymbol{w} - \boldsymbol{w}_h, p - p_h) \\ &= a(\boldsymbol{w} - \boldsymbol{w}_h, \boldsymbol{w} - \boldsymbol{v}) - b(\boldsymbol{w} - \boldsymbol{v}, p - p_h) + a_h(\boldsymbol{w}_h, \boldsymbol{v} - \boldsymbol{w}_h) - a(\boldsymbol{w}_h, \boldsymbol{v} - \boldsymbol{w}_h). \end{aligned} \tag{44}$$

By subtraction of (35) to (22), we obtain for every $q \in L_h$:

$$b(\boldsymbol{w} - \boldsymbol{w}_h, q) - \beta h^2 \left(\boldsymbol{\nabla} p_h, \boldsymbol{\nabla} q\right)_{0,\Omega} = 0, \tag{45}$$

where $\left(\boldsymbol{\nabla} p_h, \boldsymbol{\nabla} q\right)_{0,\Omega} = \int_\Omega \boldsymbol{\nabla} p_h \boldsymbol{\nabla} q dx$ denotes the scalar product in $L^2(\Omega)^d$. Consequently:

$$\begin{aligned} &b(\boldsymbol{w} - \boldsymbol{w}_h, p - p_h) + \beta h^2 \left\|\boldsymbol{\nabla}\left(p - p_h\right)\right\|_{0,\Omega}^2 \\ &= b(\boldsymbol{w} - \boldsymbol{w}_h, p - q) + \beta h^2 \left(\boldsymbol{\nabla} p, \boldsymbol{\nabla}(p - p_h)\right)_{0,\Omega} - \beta h^2 \left(\boldsymbol{\nabla} p_h, \boldsymbol{\nabla}(p - q)\right)_{0,\Omega} \end{aligned} \tag{46}$$

By adding (44), (46), and by taking into account Lemmas 3, 6 and using:

$$\begin{aligned} &|b(\boldsymbol{w} - \boldsymbol{v}, p - p_h)| \leq \|\boldsymbol{w} - \boldsymbol{v}\|_{0,\Omega} \|\boldsymbol{\nabla}(p - p_h)\|_{0,\Omega}, \\ &\|\boldsymbol{\nabla}(p_h)\|_{0,\Omega} \leq \|\boldsymbol{\nabla}(p - p_h)\|_{0,\Omega} + \|\boldsymbol{\nabla} p\|_{0,\Omega}, \end{aligned}$$

we obtain the following estimate:

$$\begin{aligned} &\|\boldsymbol{w} - \boldsymbol{w}_h\|_{1,\Omega}^2 + h^2 \left\|\boldsymbol{\nabla}\left(p - p_h\right)\right\|_{0,\Omega}^2 \\ &\leq C\Bigg(\|\boldsymbol{w} - \boldsymbol{v}\|_{1,\Omega} \|\boldsymbol{w} - \boldsymbol{w}_h\|_{1,\Omega} + \|\boldsymbol{w} - \boldsymbol{v}\|_{0,\Omega} \left\|\boldsymbol{\nabla}\left(p - p_h\right)\right\|_{0,\Omega} \\ &+ h\|\boldsymbol{w}_h\|_{1,\Omega} \|\boldsymbol{v} - \boldsymbol{w}_h\|_{1,\Omega} + \|\boldsymbol{w} - \boldsymbol{w}_h\|_{1,\Omega} \|p - q\|_{0,\Omega} \\ &+ h^2 \Bigg(\|\boldsymbol{\nabla}(p - p_h)\|_{0,\Omega} \left(1 + \|\boldsymbol{\nabla}(p - q)\|_{0,\Omega}\right) + \|\boldsymbol{\nabla}(p - q)\|_{0,\Omega} \Bigg) \Bigg), \end{aligned}$$

for every $(\boldsymbol{v},q) \in \boldsymbol{V}_h \times L_h$.

Setting $\boldsymbol{v} = \Pi_h \boldsymbol{w}$, using (28) and $q = r_h(p)$ (here $r_h : H^1(\Omega) \to L_h$ is a Clement's interpolation type; see for instance [22], $\|p - r_h(p)\|_{s,\Omega} \leq Ch^{1-s}$, $s = 0,1$) in this inequality and using the result of corollary 1, we obtain.

$$\begin{aligned} &\|\boldsymbol{w} - \boldsymbol{w}_h\|_{1,\Omega}^2 + h^2 \left\|\boldsymbol{\nabla}\left(p - p_h\right)\right\|_{0,\Omega}^2 \\ &\leq Ch\left(\|\boldsymbol{w} - \boldsymbol{w}_h\|_{1,\Omega} + h\left\|\boldsymbol{\nabla}\left(p - p_h\right)\right\|_{0,\Omega} + h \right). \end{aligned}$$

This inequality proves (42) when we set $\boldsymbol{u}_m = \boldsymbol{w}/\rho_m$ and $\boldsymbol{u}_{m,h} = \Pi_h(\boldsymbol{w}_h/\rho_m)$. □

In order to obtain an error estimate of $\|p - p_h\|_{0,\Omega}$, we proceed by duality like in [21].

Proposition 4. *Under the assumptions of Corollary 1 and (41), there exists a constant C such that*

$$\|p - p_h\|_{0,\Omega} \leq Ch. \tag{47}$$

Proof of Proposition 4. We introduce the dual problem: find $(\boldsymbol{W},Q) \in \boldsymbol{V} \times L$ satisfying

$$a(\boldsymbol{v},\boldsymbol{W}) - b(\boldsymbol{v},Q) = 0 \ \ \forall \boldsymbol{v} \in \boldsymbol{V}, \tag{48}$$

$$b(\boldsymbol{W},q) = \left(p - p_h, q\right)_{0,\Omega} \ \ \forall q \in L. \tag{49}$$

Of course we have

$$\|\boldsymbol{W}\|_{1,\Omega} + \|Q\|_{0,\Omega} \leq C\left\|p - p_h\right\|_{0,\Omega}. \tag{50}$$

By taking $q = p - p_h$ in (49) we obtain

$$\left\|p - p_h\right\|_{0,\Omega}^2 = b(\boldsymbol{W}, p - p_h) = b(\boldsymbol{W} - R_h\boldsymbol{W}, p - p_h) + b(R_h\boldsymbol{W}, p - p_h),$$

where $R_h\boldsymbol{W}$ is a Clement's interpolation of $\boldsymbol{W}$ on $\boldsymbol{V}_h$ ($\left\|\boldsymbol{W} - R_h\boldsymbol{W}\right\|_{s,\Omega} \leq Ch^{1-s}\|\boldsymbol{W}\|_{1,\Omega}$, $s = 0,1$). So we have with an integration by part:

$$\left\|p - p_h\right\|_{0,\Omega}^2 \leq Ch\left\|\boldsymbol{\nabla}\left(p - p_h\right)\right\|_{0,\Omega} \|\boldsymbol{W}\|_{1,\Omega} + \left|b(R_h\boldsymbol{W}, p - p_h)\right|$$

and by (50) and Proposition 3

$$\left\|p - p_h\right\|_{0,\Omega}^2 \leq Ch\left\|p - p_h\right\|_{0,\Omega} + \left|b(R_h\boldsymbol{W}, p - p_h)\right|. \tag{51}$$

It remains to estimate $\left|b(R_h\boldsymbol{W}, p - p_h)\right|$.

Relation (43) with Lemma 6 implies

$$\begin{aligned} \left|b(R_h\boldsymbol{W}, p - p_h)\right| &\leq \left|a(\boldsymbol{w} - \boldsymbol{w}_h, R_h\boldsymbol{W})\right| + \left|a_h\left(\boldsymbol{w}_h, R_h\boldsymbol{W}\right) - a\left(\boldsymbol{w}_h, R_h\boldsymbol{W}\right)\right| \\ &\leq C\|\boldsymbol{w} - \boldsymbol{w}_h\|_{1,\Omega} \|R_h\boldsymbol{W}\|_{1,\Omega} + Ch\|\boldsymbol{w}_h\|_{1,\Omega} \|R_h\boldsymbol{W}\|_{1,\Omega} \\ &\leq Ch\|\boldsymbol{W}\|_{1,\Omega}. \end{aligned}$$

This last estimate with (50) and (51) leads to the conclusion. □

Remark 3. By the same procedure of duality, one can obtain an estimate for $\|\boldsymbol{u}_m - \boldsymbol{u}_{m,h}\|_{0,\Omega}$. However, this requires the uniqueness and sufficient regularity on the solutions of a dual problem.

Proposition 5. *Under the hypothesis of Proposition 4, and if $\boldsymbol{u}_g \in H^2(\Omega)^d$, there exists a constant C independent of $h \leq h_0$ such that*

$$\left\|\boldsymbol{u}_g - \boldsymbol{u}_{g,h}\right\|_{1,\Omega} \leq Ch. \tag{52}$$

Proof. Setting:

$$f(\boldsymbol{v}) = \int_\Omega p\nabla\alpha_g.\boldsymbol{v} dx + \int_\Omega \alpha_g p \operatorname{div}(\boldsymbol{v}) dx + \int_\Omega (\alpha_g\rho_g\, \boldsymbol{g} + D\frac{\alpha_g\rho}{\rho_l}\boldsymbol{u}).\boldsymbol{v} dx,$$

and

$$f_h(\boldsymbol{v}) = \int_\Omega p_h\nabla\alpha_g.\boldsymbol{v} dx + \int_\Omega \alpha_g p_h \operatorname{div}(\boldsymbol{v}) dx + \int_\Omega (\alpha_g\rho_g\, \boldsymbol{g} + D\frac{\alpha_g\rho}{\rho_l}\boldsymbol{u}_h).\boldsymbol{v} dx,$$

we have

$$\begin{aligned} \left|f(\boldsymbol{v}) - f_h(\boldsymbol{v})\right| &\leq C\{\|p - p_h\|_{0,\Omega} \left\|\alpha_g\right\|_{1,3,\Omega} \|\boldsymbol{v}\|_{0,6,\Omega} \\ &+ \|p - p_h\|_{0,\Omega} \|\boldsymbol{v}\|_{1,\Omega} + \|\boldsymbol{u} - \boldsymbol{u}_h\|_{0,\Omega} \|\boldsymbol{v}\|_{0,\Omega}\} \end{aligned} \tag{53}$$

and a consequence of Propositions 3 and 4 is that

$$\left|f(\boldsymbol{v}) - f_h(\boldsymbol{v})\right| \leq Ch\|\boldsymbol{v}\|_{1,\Omega} \ \ \forall \boldsymbol{v} \in \boldsymbol{V}. \tag{54}$$

Thanks to the continuous and bilinear form $l(.,.)$(24), we can write Problems (15) and (31), as

$$l(\boldsymbol{u}_g, \boldsymbol{v}) = f(\boldsymbol{v}) \ \ \forall \boldsymbol{v} \in \boldsymbol{V}, \tag{55}$$

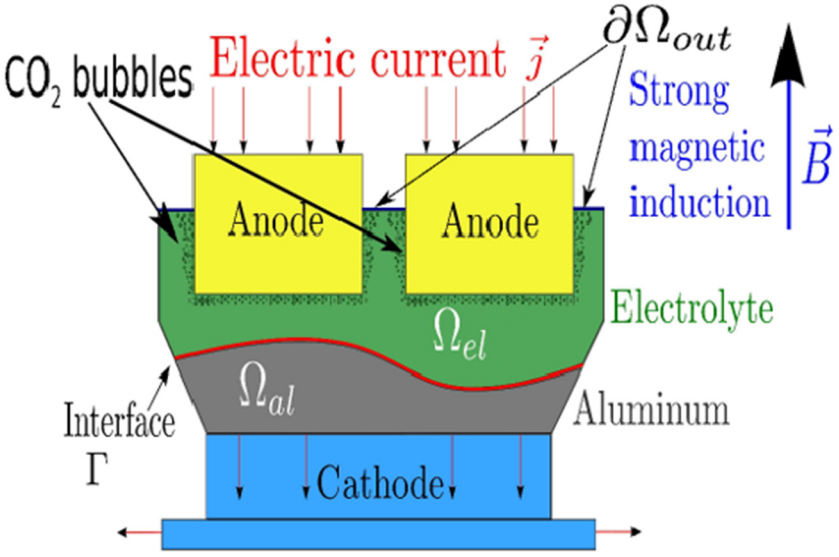

Fig. 1. Vertical cut of an electrolysis cell.

and

$$l(\boldsymbol{u}_{g,h}, \boldsymbol{v}) = f_h(\boldsymbol{v}) \quad \forall \boldsymbol{v} \in \boldsymbol{V}_h. \tag{56}$$

Of course we have $l(\boldsymbol{u}_g - \boldsymbol{u}_{g,h}, \boldsymbol{v}) = f(\boldsymbol{v}) - f_h(\boldsymbol{v})$, $\forall \boldsymbol{v} \in \boldsymbol{V}_h$, and if $\boldsymbol{u}_g \in H^2(\Omega)^3$:

$$\begin{aligned} &\left|l(\boldsymbol{u}_g - \boldsymbol{u}_{g,h}, \boldsymbol{u}_g - \boldsymbol{u}_{g,h})\right| = \left|l(\boldsymbol{u}_g - \boldsymbol{u}_{g,h}, \boldsymbol{u}_g - \boldsymbol{v}) + l(\boldsymbol{u}_g - \boldsymbol{u}_{g,h}, \boldsymbol{v} - \boldsymbol{u}_{g,h})\right| \\ &\leq \left|l(\boldsymbol{u}_g - \boldsymbol{u}_{g,h}, \boldsymbol{u}_g - \boldsymbol{v})\right| + \left|f(\boldsymbol{v} - \boldsymbol{u}_{g,h}) - f_h(\boldsymbol{v} - \boldsymbol{u}_{g,h})\right|. \end{aligned} \tag{57}$$

Taking $\boldsymbol{v} = \Pi_h(\boldsymbol{u}_g)$ and using (54), we finally have

$$l(\boldsymbol{u}_g - \boldsymbol{u}_{g,h}, \boldsymbol{u}_g - \boldsymbol{u}_{g,h}) \leq Ch\left(\left\|\boldsymbol{u}_g - \boldsymbol{u}_{g,h}\right\|_{1,\Omega} + \left\|\Pi_h \boldsymbol{u}_g - \boldsymbol{u}_{g,h}\right\|_{1,\Omega}\right).$$

With the coercivity of $l(.,.)$ on $\boldsymbol{V} \times \boldsymbol{V}$ we obtain the conclusion. □

5. Numerical experiments

In this section, we present two numerical experiments, the first one is to check convergence of the finite element method (29) (30) corresponding to the simplified problem in the unit cube, the density ρ_m being prescribed. Second, we show an example of industrial application pertaining to aluminium electrolysis, the complete model (3) (4) (6) (8) being considered.

5.1. Convergence for the simplified problem

Eqs. (10) (11) are solved with the finite element scheme (29) (30) and implemented with Fenics [23]. The unit cube $\Omega = (0,1)^3$ is cut in tetrahedrons with $N \times N \times N$ vertices. The volume fraction of gas is given by

$$\alpha_g(x_1, x_2, x_3) = \frac{1}{2}\left(1 + \tanh\left(\gamma\left(x_3 - \frac{1}{2}\right)\right)\right).$$

We set $\rho_b = 1$, thus when $\rho_g = 1$ then the mixture density ρ_m defined by (1) is constant and when $\rho_g = 0.5$, then the mixture density varies in Ω. The mixture velocity is given by:

$$\boldsymbol{u}_m(x_1, x_2, x_3) = \frac{1}{\rho_m(x_1, x_2, x_3)} \begin{pmatrix} (4(2x_2x_3 - x_2 - x_3 + 1))(x_2 - 1)x_2(x_1 - 1)^2(-x_3 + x_2)(x_3 - 1)x_1^2x_3 \\ -4(x_2 - 1)^2(-x_3 + x_1)x_2^2(x_1 - 1)(2x_1x_3 - x_1 - x_3 + 1)(x_3 - 1)x_1x_3 \\ (4(x_2 - 1))x_2(-x_2 + x_1)(x_1 - 1)(2x_1x_2 - x_1 - x_2 + 1)(x_3 - 1)^2x_1x_3^2 \end{pmatrix},$$

so that $\mathrm{div}(\rho_m \boldsymbol{u}_m) = 0$ and $\boldsymbol{u}_m = 0$ on $\partial\Omega$, the zero mean pressure is defined by:

$$p(x_1, x_2, x_3) = 1\left(x_1x_2x_3 - \frac{1}{8}\right), \tag{58}$$

and we replace the right hand side of (10) by the appropriate force term.

Convergence is checked by computing the errors and convergence rates defined by:

$$e_i(m) = \left\|m - m_h\right\|_{i,\Omega}, \; r_i(m) = \frac{\log\left(e_i(m)/\hat{e}_i(m)\right)}{\log(h/\hat{h})},$$

where m is either the velocity or pressure, $i \in \{0,1\}$, e and $\hat{e}$ denote the errors computed on two consecutive meshes of size h and $\hat{h}$. The number of iterations required to solve the linear system with GMRES is denoted as N_{iter}. The results are reported in Tables 1 and 2 when $\gamma = 10$. The convergence rates seem to be slightly better than those proved in Section 4, namely one. As expected, the number of GMRES iterations is doubled when h is halved (N is doubled).

Table 1
Convergence rates for the simplified model with constant density ($\rho_g = 1$).

N	$e_0(p)$	$r_0(p)$	$e_1(u_m)$	$r_1(u_m)$	N_{iter}
10	2.1659e−03	–	1.4218e−03	–	16
20	8.6205e−04	1.33	7.6989e−04	0.89	33
40	4.8304e−04	0.841	4.2899e−04	0.84	74
80	2.0911e−04	1.21	2.0311e−04	1.08	185
160	7.4389e−05	1.49	8.9891e−05	1.18	497

Table 2
Convergence rates for the simplified model with variable density ($\rho_g = 0.5$).

N	$e_0(p)$	$r_0(p)$	$e_1(u_m)$	$r_1(u_m)$	N_{iter}
10	2.4480e−03	–	2.1377e−03	–	15
20	1.3048e−03	0.91	1.2394e−03	0.79	32
40	8.0283e−04	0.70	7.1062e−04	0.80	72
80	3.5774e−04	1.17	3.3891e−04	1.07	185
160	1.2689e−04	1.50	1.4733e−04	1.20	521

5.2. Industrial application to an electrolysis cell

Our purpose is now to simulate the stationary mixture velocity in an electrolysis cell. The unknowns are the velocity of the mixture $\boldsymbol{u}_m$, the pressure p, the velocity of the gas $\boldsymbol{u}_g$ and the gas distribution α_g, the equations are (3) (4) (6) (8). Numerical investigations have shown

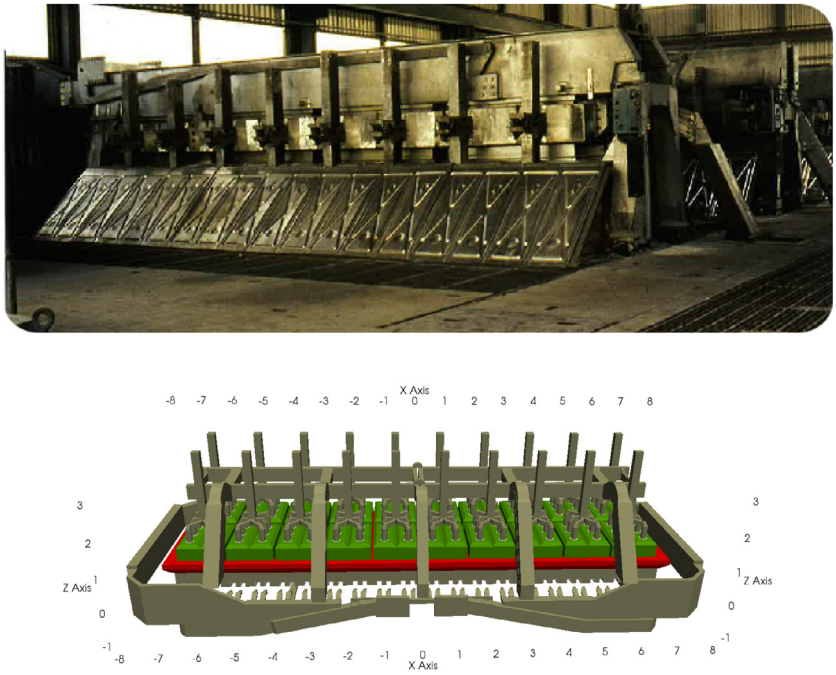

Fig. 2. Top: industrial cell (courtesy of Rio Tinto Aluminium[2]) and bottom the corresponding mesh. The grey structure allows the electric current to reach the anodic blocks (green) then the fluid domain Ω (in red). The dimensions of Ω are about 14 [m] × 4 [m] × 35 [cm].

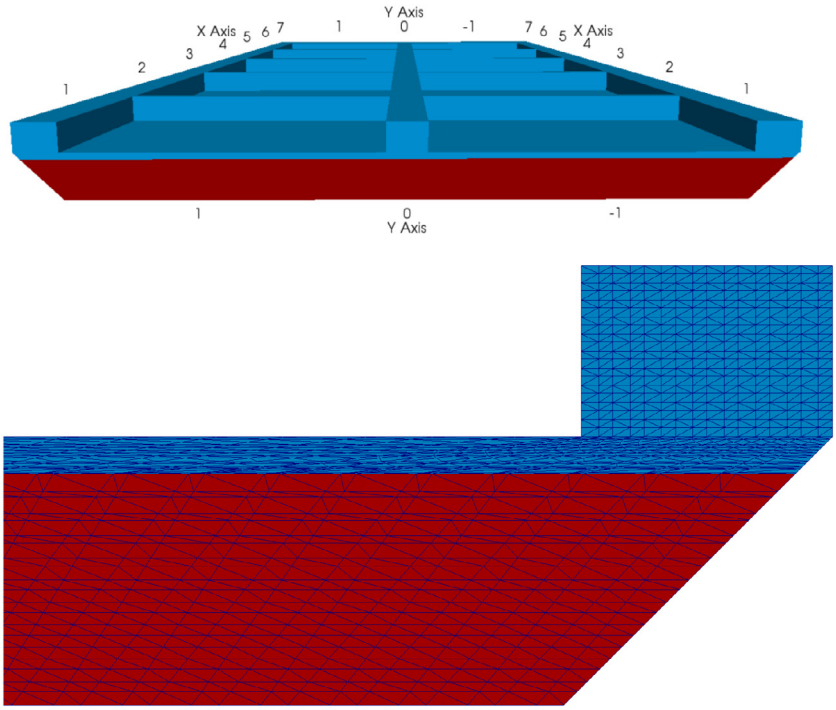

Fig. 3. Vertical cut at x = 0.5 [m]: the computational domain of the fluid is composed of the electrolytic bath Ω_{el} (in blue), corresponding to a thin layer under the anodes, as well as the volume in the different channels surrounding the anodic blocks, and the liquid aluminium Ω_{al} (in red) beneath.

that an efficient strategy is to perform one time step of (8) in order to obtain a new α_g, then to solve the stationary equations corresponding to (3) (4) (6) to obtain $\boldsymbol{u}_m$, p and $\boldsymbol{u}_g$, which is a well posed problem provided α_g is small enough. In practice, we solve (8) from time 0 to 100$[s]$ with a Euler scheme and timestep 0.1$[s]$, starting from $\alpha_g = 0$. A Smagorinski law [14,24] is used to model turbulence in the viscosities μ_m, μ_g, and in the diffusivity coefficient k. Given the new α_g, a few Newton iterations then suffice to solve the nonlinearities in (3) (4) (6). The coefficient modelling the drag force D corresponds to Stokes' law, i.e $D = 18\mu_m/d^2$, with $d = 4$ [mm] the average diameter of the gas bubbles [25]. The generation of gas in the bath is modelled by the source term $\dot{\alpha}_g$ in (8), which is computed from the total production of CO_2 getting out of the cell. In standard conditions, $\dot{\alpha}_g = S_0$, where

[2] In "Cinquante ans de recherches sur la production d'aluminium au LRF", Mauve Carbonell, Ivan Grinberg and Maurice Laparra, 2012

(a) Volume fraction of gas α_g in the middle of the bath (plane $z = 0.216[m]$) and in a profile view (plane $x = 0.5[m]$)

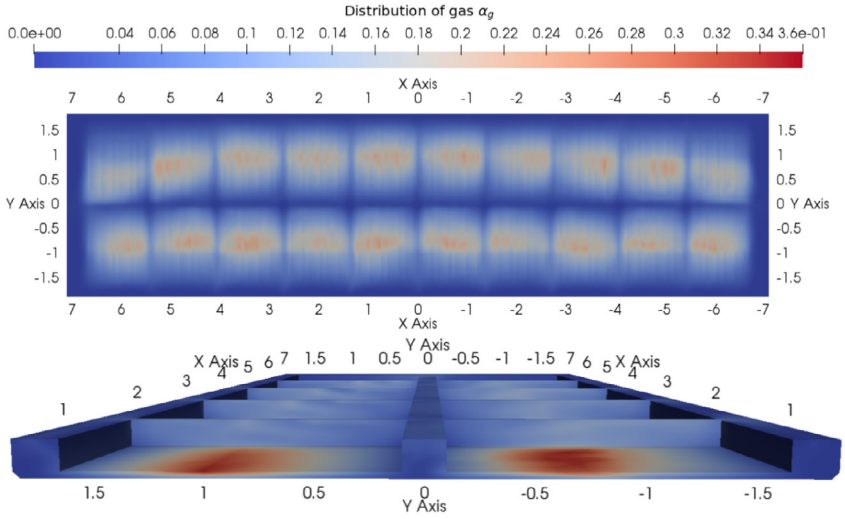

(b) Velocity field $\boldsymbol{u}_m$ in the middle of the bath ($z = 0.216[m]$) and streamlines

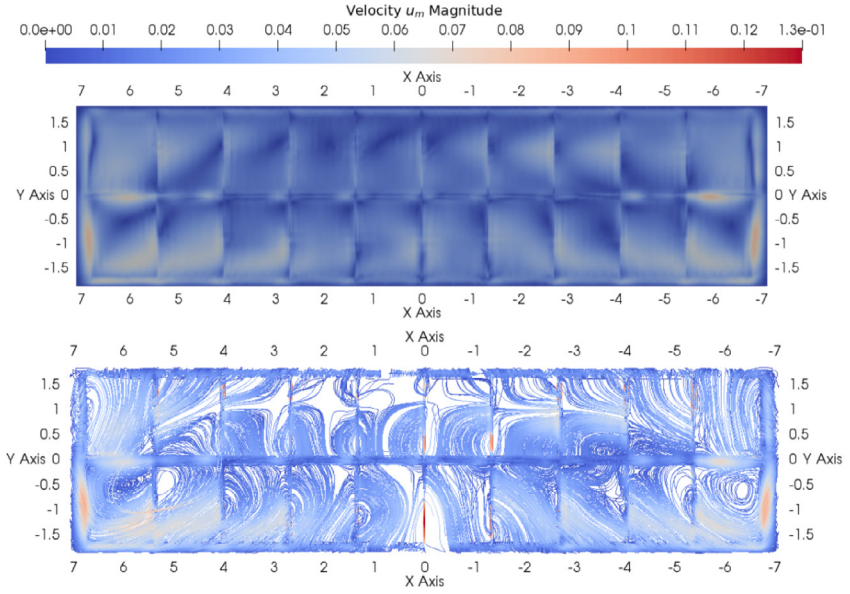

Fig. 4. Distribution of gas α_g and velocity field $\boldsymbol{u}_m$ when $\dot{\alpha}_g = S_0$.

S_0 corresponds to the production of CO_2 due to Faraday's law on the whole cell:

$$\int_\Omega S_0 dx = \int_{\partial\Omega} \frac{\boldsymbol{j}\cdot\boldsymbol{n} M_{CO_2}}{4\mathcal{F}\rho_g} ds, \tag{59}$$

$\boldsymbol{j}$ being the current density [A/m^2], $M_{CO_2} = 44.01$ [g/mol] is carbon dioxide molar mass and $\mathcal{F}$ is Faraday's constant. In our simulations we have considered that S_0 is proportional to div $\boldsymbol{j}$, where $\boldsymbol{j}$ is computed using the Alucell software [9,14]. Simulations are shown when $\dot{\alpha}_g = 0, S_0/2, S_0, 2S_0$. According to the existence and convergence theory of Sections 3 and 4, if α_g is small enough and if it remains in the $[0, 1]$ interval, then we expect that the velocities converge with respect to the mesh size. However, since we are using finite elements, there is no maximum principle for α_g, moreover, we do not know what "small enough" means in this industrial context. In this simulation, we have not been able to obtain stationary solutions when the source term $\dot{\alpha}_g$ is larger than $2S_0$.

During aluminium electrolysis, a two fluids interface problem is involved [3,9,26], the aluminium domain Ω_{al} and the so-called electrolytic bath domain Ω_{el}, see Fig. 1 for notations. The chemical reaction between alumina and carbon

$$2Al_2O_3 + 3C => 3CO_2 + 4Al$$

occurs in the electrolytic bath only, it produces bubbles of carbon dioxide. Here, the two fluids interface problem is disregarded, the interface between Ω_{al} and Ω_{el} is assumed to be flat. Strong electromagnetic forces apply to these two domains, the force term $\boldsymbol{F}$ in (3). These forces are again computed using the Alucell software [9,14].

The industrial cell and the corresponding mesh are shown in Fig. 2. The domains Ω_{al} and Ω_{el} are shown in Fig. 3. The electrolytic bath in blue consists of a thin layer of only 3.2 [cm] between the interface to the anodes, while the liquid aluminium in red represents a thicker layer of 20 [cm] beneath. The top of the electrolytic bath corresponds to $\partial\Omega_{out}$ in Fig. 1 and is located 18 [cm] above the interface. The blocks correspond to the anodes that are immersed in the bath.

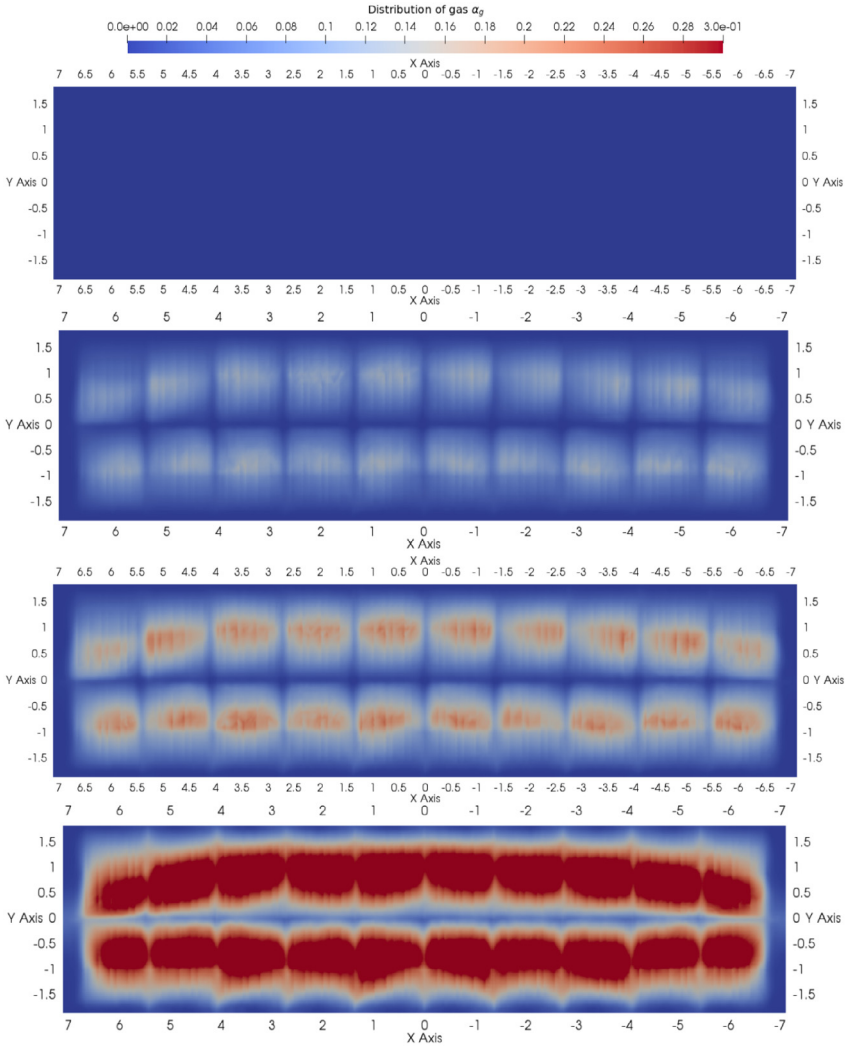

Fig. 5. Volume fraction of gas α_g in the middle of the bath (plane $z = 0.216$ [m]) with $\dot{\alpha}_g = 0.0, S_0/2, S_0, 2S_0$.

The mixture velocity $\boldsymbol{u}_m$ and the pressure p are solved in the whole fluid domain $\Omega_{al} \cup \Omega_{el}$, while the gas velocity $\boldsymbol{u}_g$ and gas fraction α_g are assumed to be zero in the aluminium domain and are only solved in the electrolytic bath Ω_{el}. The boundary condition for the volume fraction of gas is:

$$k\frac{\partial \alpha_g}{\partial n} = 0 \text{ on } \partial\Omega_{el},$$

those for the mixture velocity are slip boundary conditions:

$$\boldsymbol{u}_m \cdot \boldsymbol{n} = 0 \text{ and } \left(\boldsymbol{\sigma}_m \cdot \boldsymbol{n}\right) \cdot t_i = 0,\ i = \{1,\ 2\} \text{ on } \partial(\Omega_{al} \cup \Omega_{el}),$$

those for the gas velocity $\boldsymbol{u}_g$ are slip boundary condition, except zero force on the top:

$$\boldsymbol{u}_g \cdot \boldsymbol{n} = 0 \text{ and } \left(\boldsymbol{\tau}_g - p\alpha_g \boldsymbol{I}\right) \cdot \boldsymbol{n} \cdot t_i = 0,\ i = \{1,\ 2\} \text{ on } \partial\Omega_{el} \setminus \partial\Omega_{out},$$
$$\left(\boldsymbol{\tau}_g - p\alpha_g \boldsymbol{I}\right) \cdot \boldsymbol{n} = 0 \text{ on } \partial\Omega_{out}.$$

Fig. 4 shows the volume fraction of gas α_g and the velocity field $\boldsymbol{u}_m$ corresponding a simulation with $\dot{\alpha}_g = S_0$. The gas clearly accumulates under the anodes. Fig. 5 shows the volume fraction of gas α_g in the middle of the bath when $\dot{\alpha}_g = 0.0,\ S_0/2,\ S_0$ and $2S_0$. The corresponding velocity fields are shown in Fig. 6. The discrepancy of the mixture velocity is computed when $\dot{\alpha}_g = 0$ and $\dot{\alpha}_g = S_0$. It is 14% in the aluminium domain, 46% in the electrolytic bath below the anodes and 95% in the channels between the anodes. We therefore conclude that the bubbles of gas have a tremendous influence on the fluid flow in the channels between the anodes. This will certainly have strong influences on alumina transport [27,28], therefore on the overall process efficiency.

6. Conclusion

A model to take into account the influence of gas bubbles in aluminium electrolysis is presented. Since the gas bubbles (carbon dioxide) are small (millimetres) and the electrolysis cell is large (metres), gas is assumed to be a dilute dispersion in the liquid (the electrolytic bath). The model has four unknowns, the mixture velocity, the gas velocity, the pressure and the volume fraction of gas. The equations are derived from mass and momentum conservation of the mixture and of the gas.

A simplified model is considered when the volume fraction of gas is known. It is proved that, in the stationary case, when the convective terms are disregarded and provided the volume fraction of gas is small enough, the remaining set of equations is well posed. Convergence of a finite element scheme is also proved.

Numerical results are reported for the simplified model and for the complete model. Industrial simulations indicate that the effect of gas on the mixture flow cannot be disregarded.

From the theoretical point of view, well-posedness of the complete model should be investigated, so as well-posedness of the simplified problem when the volume fraction is large. Adaptive methods should also be investigated, since refinement in specific regions of the cell

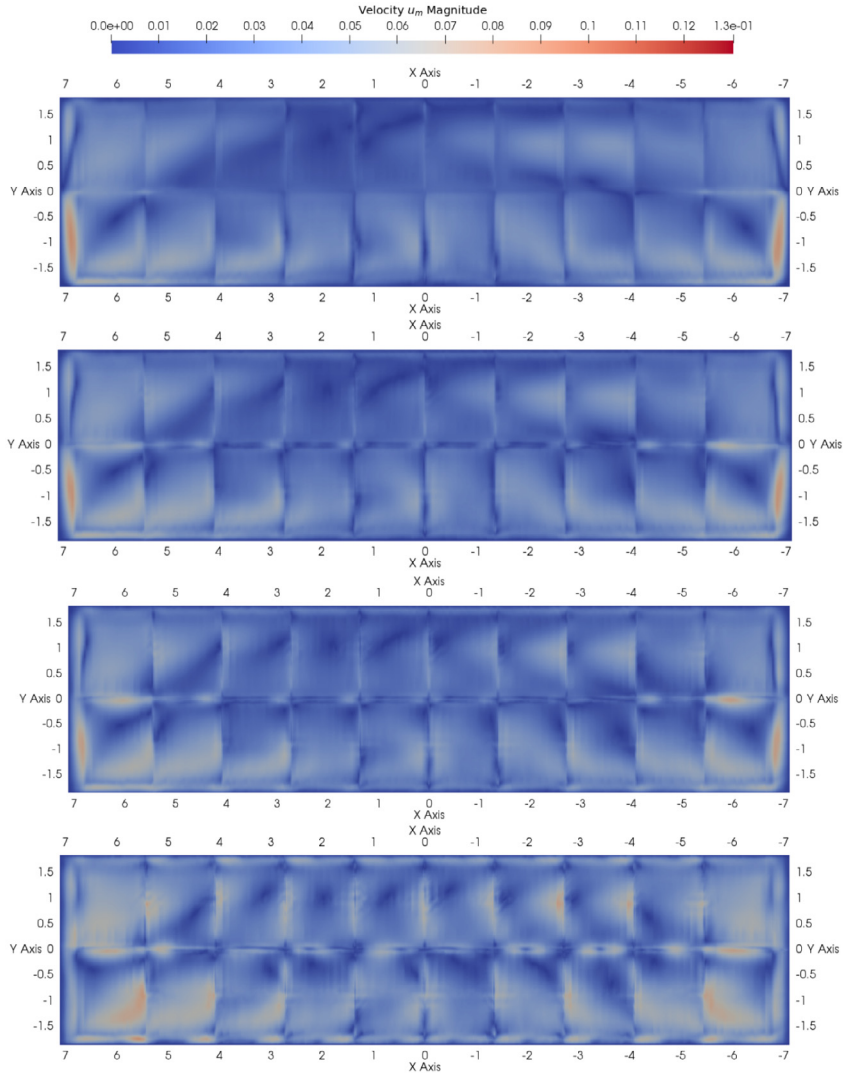

Fig. 6. Amplitude of the velocity field $\boldsymbol{u}_m$ obtained in the middle of the bath (plane $z = 0.216$ [m]) with $\dot{\alpha}_g = 0.0, S_0/2, S_0, 2S_0$.

seems to be unavoidable. From the industrial point of view, the coupling of the presented model with electromagnetic and thermal effects should be investigated.

Acknowledgements

Emile Soutter is financed by the Rio Tinto Aluminium LRF Research Center at Saint Jean de Maurienne. All the team of Rio Tinto Aluminium LRF in Saint-Jean de Maurienne is acknowledged for support.

References

[1] S. Das, Achieving carbon neutrality in the global aluminum industry, JOM 64 (2012) http://dx.doi.org/10.1007/s11837-012-0237-0.

[2] M. Dupuis, V. Bojarevics, Weakly coupled thermo-electric and mhd mathematical models of an aluminium electrolysis cell, Light Metals 1 (2005) 449–454.

[3] J.-F. Gerbeau, C. Bris, T. Lelièvre, Mathematical methods for the magnetohydrodynamics of liquid metals, Math. Methods Magnetohydrodyn. Liquid Metals (2006) http://dx.doi.org/10.1093/acprof:oso/9780198566656.001.0001.

[4] K.E. Einarsrud, I. Eick, W. Bai, Y. Feng, J. Hua, P.J. Witt, Towards a coupled multi-scale, multi-physics simulation framework for aluminium electrolysis, Appl. Math. Model. 44 (2017) 3–24, http://dx.doi.org/10.1016/j.apm.2016.11.011.

[5] M. Sun, B. Li, L. Li, Multiscale simulation of bubble behavior in aluminum reduction cell using a combined discrete-bubble-model-volume-of-fluid-magnetohydrodynamical method, Ind. Eng. Chem. Res. 58 (8) (2019) 3407–3419, http://dx.doi.org/10.1021/acs.iecr.8b05109.

[6] F. Panescu, Modelisation Eulerienne d'ecoulements diphasiques a phase dispersee et simulation numerique par une methode volumes - elements finis, (PhD thesis), Université de Nice Sophia Antipolis, 2006, URL http://scholar.google.com/scholar?hl=en{&}btnG=Search{&}q=intitle:par+Modelisation+Eulerienne+d+?ecoulements+diphasiques+a+phase+dispersee+et+simulation+numerique+par+une+methode+volumes+-+elements+finis{#}0.

[7] R. Ruiz-Baier, I. Lunati, Mixed finite element - discontinuous finite volume element discretization of a general class of multicontinuum models, J. Comput. Phys. 322 (2016) 666–688, http://dx.doi.org/10.1016/j.jcp.2016.06.054, URL http://www.sciencedirect.com/science/article/pii/S0021999116302790.

[8] S. Zhan, Z. Wang, J. Yang, R. Zhao, C. Li, J. Wang, J. Zhou, 3D numerical simulations of gas-liquid two-phase flows in aluminum electrolysis cells with the coupled model of computational fluid dynamics-population balance model, Ind. Eng. Chem. Res. 56 (30) (2017) 8649–8662, http://dx.doi.org/10.1021/acs.iecr.7b01765.

[9] G. Steiner, Simulation numérique de phénomènes MHD: Application à l'électrolyse de l'aluminium (PhD thesis NO 4469 EPFL), 2009, http://dx.doi.org/10.5075/epfl-thesis-4469, URL https://infoscience.epfl.ch/record/138750/files/EPFL{_}TH4469.pdf.

[10] M. Flueck, T. Hofer, A. Janka, J. Rappaz, Numerical methods for ferromagnetic plates, Comput. Methods Appl. Sci. 15 (2010) 169–182, http://dx.doi.org/10.1007/978-90-481-3239-3_13.

[11] S. Renaudier, S. Langlois, B. Bardet, M. Picasso, A. Masserey, Alucell: A unique suite of models to optimize pot design and performance, in: TMS Annual Meeting & Exhibition, Springer, 2018, pp. 541–549, http://dx.doi.org/10.1007/978-3-319-72284-9_71.

[12] S. Langlois, J. Rappaz, O. Martin, Y. Caratini, M. Flueck, A. Masserey, G. Steiner, 3D coupled MHD and thermo-electrical modelling applied to AP technology pots, in: Light Metals 2015, Springer, 2015, pp. 771–775, http://dx.doi.org/10.1007/978-3-319-48248-4_130.

[13] B. Bardet, T. Foetisch, S. Renaudier, J. Rappaz, M. Flueck, M. Picasso, Alumina dissolution modeling in aluminium electrolysis cell considering MHD driven convection and thermal impact, in: Light Metals 2016, Springer, 2016, pp. 315–319, http://dx.doi.org/10.1007/978-3-319-48251-4_52.

[14] J. Rochat, Approximation numérique des écoulements turbulents dans des cuves d'électrolyse de l'aluminium (PhD thesis NO 7113 EPFL), 2016, http://dx.doi.org/10.5075/epfl-thesis-7113, URL https://infoscience.epfl.ch/record/221291/files/EPFL{_}TH7113.pdf.

[15] G. Caloz, J. Rappaz, Numerical analysis for nonlinear and bifurcation problems, in: Handbook of Numerical Analysis, Vol. 5, 1997, pp. 487–637, http://dx.doi.org/10.1016/S1570-8659(97)80004-X.

[16] G.N. Gatica, R. Oyarzúa, R. Ruiz-Baier, Y.D. Sobral, Banach spaces-based analysis of a fully-mixed finite element method for the steady-state model of fluidized beds, Comput. Math. Appl. 84 (2021) 244–276.

[17] C. Bernardi, F. Laval, B. Metivet, B. Pernaud-thomas, Finite element approximation of viscous flow with varying density, SIAM J. Numer. Anal. 29 (5) (1992) 1203–1243, http://dx.doi.org/10.1137/0729073.

[18] A. Ern, Vorticity-velocity formulation of the Stokes problem with variable density and viscosity, Math. Models Methods Appl. Sci. 8 (1996) 203–218, http://dx.doi.org/10.1142/S021820259800010X.

[19] V. Girault, P.-A. Raviart, Finite element methods for Navier-Stokes equations: Theory and algorithms, first ed., Springer Publishing Company, Incorporated, 2011, http://dx.doi.org/10.1007/978-3-642-61623-5.

[20] P.G. Ciarlet, Finite Element Method for Elliptic Problems, Society for Industrial and Applied Mathematics, USA, 2002.

[21] F. Brezzi, J. Douglas, Stabilized mixed methods for the Stokes problem, Numer. Math. 53 (1–2) (1988) 225–235, http://dx.doi.org/10.1007/BF01395886.

[22] P. Clément, Approximation by finite element functions using local regularization, ESAIM: Math. Model. Numer. Anal. Modél. Math. Anal. Numér. 9 (R2) (1975) 77–84, http://dx.doi.org/10.1051/m2an/197509r200771, URL http://www.numdam.org/item/M2AN_1975_9_2_77_0.

[23] M. Alnæs, J. Blechta, J. Hake, A. Johansson, B. Kehlet, A. Logg, C. Richardson, J. Ring, M. Rognes, G. Wells, The fenics project version 1.5, Arch. Numer. Softw. 3 (100) (2015) http://dx.doi.org/10.11588/ans.2015.100.20553.

[24] S.B. Pope, Turbulent flows, Meas. Sci. Technol. 12 (11) (2001) http://dx.doi.org/10.1088/0957-0233/12/11/705.

[25] S. Poncsák, Formation et évolution des bulles de gaz au-dessous de l'anode dans une cuve d électrolyse d'aluminium (PhD thesis Université du Québec), 2000, http://dx.doi.org/10.1522/12270309.

[26] J. Descloux, R. Frosio, M. Flueck, A two fluids stationary free boundary problem, Comput. Methods Appl. Mech. Engrg. 77 (1989) 215–226, http://dx.doi.org/10.1016/0045-7825(89)90076-5.

[27] T. Hofer, Numerical Simulation and Optimization of the Alumina Distribution in an Aluminium Electrolysis Pot (PhD thesis NO 5023 EPFL), 2011, http://dx.doi.org/10.5075/epfl-thesis-5023, URL https://infoscience.epfl.ch/record/164017/files/EPFL{_}TH5023.pdf.

[28] T.F. Hilke, Méthodes numériques liées à la distribution d'alumine dans une cuve d'électrolyse d'aluminium (PhD thesis NO 8682 EPFL), 2019, http://dx.doi.org/10.5075/epfl-thesis-8682, URL http://infoscience.epfl.ch/record/265157.